Nigerian Journal of Engineering, Vol. 29, No. 1, April 2022, ISSN (print): 0794 – 4756, ISSN(online):2705-3954.

Nigerian Journal of Engineering,
Faculty of Engineering, Ahmadu Bello University, Zaria, Nigeria
journal homepage: www.njeabu.com.ng

Hardness Characteristics of AISI 1020 Low Carbon Steel Weldment Produced by Tungsten Inert Gas Welding

I. B. Owunna, A. E. Ikpe*

Department of Mechanical Engineering, University of Benin, Benin City, PMB 1154.
*aniekan.ikpe@eng.uniben.edu

Research Article

Abstract

The present study investigates the post-weld characteristics of AISI 1020 low carbon steel weldment produced by Tungsten Inert Gas (TIG) welding at distinct arc current steps. Scanning Electron Microscopy (SEM) was used for imaging the microstructure and morphology of the welds while Energy Dispersive Spectroscopy (EDS) was employed in checking the mechanical properties and characterization of the weld. LECO micro-hardness tester with a load of 150 kg was used in determining the Rockwell Hardness Number of each welded sample. Increased welding current led to increase in the arc heat, causing the grains to recrystallize and increase in sizes, as such, reducing hardness of the weldment and the Heat Affected Zone (HAZ). At welding current of 96.14, 120, 155, 190 and 213A, hardness values of 176.3, 164.2, 136.4, 112.5 and 93.6 were obtained from the fusion zone of each welded specimen while hardness values of 192.2, 174.3, 144.6, 124.8 and 106.3 were obtained from the HAZ of each welded specimen. However, the base metal was not affected as uniform hardness of 115.2 was observed for all the welded samples due to the absence of arc heat disorienting the atoms in the metal lattice.

Keywords
TIG welding, Low carbon steel, Rockwell hardness, Microstructure, Arc heat.

Article History
Received: – June, 2021
Reviewed: – December, 2021,
Accepted: – April, 2022
Published: – April, 2022

1. Introduction

Tungsten Inert Gas (TIG) welding is a welding technique that is applicable in the fusion of metals together via arc heating between a non-consumable electrode (EWTh2) and the welded specimen (Ravichandran *et al.*, 2017), while the welding process is shielded by inert gas such as argon or helium to prevent atmospheric contamination of the molten weld pool (Srirangan and Paulraj, 2015). Microstructure as well as the mechanical properties of welded sample such as yield strength, toughness and Rockwell hardness etc. are usually assessed in order to ascertain the integrity and suitability of the weld for industrial applications (Ikeh *et al.*, 2019).

Joshi et al. (2016) employed TIG welding and laser beam welding (LBW) technique in the fusion of two dissimilar metals which included 18% Ni maraging steel 250 and AISI 4130 steel. Welds integrity were examined through tensile testing, optical microstructures and micro-hardness test. The LBW welds produced good mechanical properties and low HAZ compared to welds produced from TIG welding. In addition, the LBW process improved the integrity of the welds from 62% to 97% in terms of ultimate tensile strength. Kumar and Sunderrajan (2009) investigated the process parameter effects of pulsed TIG welding on mechanical properties of AL-Mg-Si alloy. Values obtained for hardness increased significantly in the HAZ due to the presence of fine grain at welding current of 200A compared to the low hardness values obtained in the fusion zone. The microstructure consisted primarily of dendrites with arm spacing equal to the grain size. Hardness and microstructure of mild steel joint produced by TIG welding technique were investigated by Uduehiabhulimen (2014). The weld joint had the highest hardness values followed by the HAZ and finally the base metal. For the welding process parameters, current was also noted to contribute mostly to the effect of hardness values. Ikpe et al. (2017) investigated the effects of welding current and arc voltage on TIG welding arc length for 10mm mild steel plate. From result of the findings, higher welding current and arc voltage resulted in weld beads that are longer and wider, which signifies poor weld quality. Badheka *et al.* (2016) evaluated the microstructural characteristics of AISI 304 stainless steel as well as carbon steel joined by TIG and activated flux-TIG (A-TIG) welding techniques. Widmanstatten ferrite structure was observed at the HAZ of the A-TIG welded carbon steel material while there were variations in the microstructure at the fusion zone of stainless steel and using the two welding techniques. Microstructures revealed significant heterogeneity in grain particles as well as grain disorientations. Ishak *et al.* (2015) investigated the effect of filler on weld metal structure of AA6061 aluminum alloy using TIG welding process. The welded specimen was butt joined with three different fillers: ER5356 (4.5-6% Mg), ER4043 (4.5–6% Si) and ER4047 (11–13% Si). Effects of these fillers on the welds were analyzed by their hardness, microstructures, visual appearance as well as yield strength. A fine grain size microstructure with yield strength of 171.53 MPa was obtained with ER5356 compared to weld joints using ER4047 and ER4047 fillers which produced yield strength values of

167.34MPa and 168.03 MPa and somewhat coarse grain sizes. Singh *et al.* (2016) investigated the microstructural and hardness variations in En31 steel and mild steel joints produced from TIG welding technique. The test results obtained for maximum hardness were 490 HV and 498 HV for both steel materials at welding current of 150 A and gas flow rate of 7 L/min. Ravichandran et al. (2017) employed Signal to noise (SN) ratio and Analysis of Variance (ANOVA) in analyzing TIG welding to determine the optimum process parameters for joining duplex stainless steel (2205) plates. Welding current, gas flow rate and welding speed were considered as the welding parameters and impact strength and hardness were taken as responses. The studies revealed that high impact strength can be obtained with welding current, gas flow rate and welding speed of 150 A, 14 L/min and 210 mm/min. Moreover, increase in hardness of the weld was obtained at welding current, gas flow rate and welding speed of 190 A, 12L/min and 175 mm/min. Images obtained from Scanning Electron Microscopy (SEM) for the base metal and fusion zone region indicated dendrite structure. Cibi and Thilagham (2017) compared the variants of Gas Tungsten Arc Welding (GTAW) technique including pulsed GTAW, conventional GTAW and GTAW with high frequency for surface finishing of mild steel fillet welded plate. The results were examined using microstructural test and surface hardness which revealed that the base metal and weld metal were of similar ferrite and pearlite composition while the formation of acicular ferrite was an indication of improvement in toughness of the material. Hardness in the conventional GTAW finishing and conventional GTAW with High frequency dressed specimen had the most desired hardness profile with adequate uniformity in the hardness across the material thickness.

Understanding of material properties and characteristics is a major challenge that can result in poor performance of engineering structures due to improper tests and experiments as well as the right welding method/procedures to determine whether or not the properties/characteristics of a given material can withstand the service condition it is meant to be subjected to. In this study, hardness characteristics of AISI 1020 low carbon steel weldment produced by tungsten inert gas welding was investigated. Analysis of the welds of AISI 1020 low carbon steel plates was carried out to determine the microstructural properties and hardness characteristics of the parent metals, HAZ, and the fusion zones. Findings of the study will enable engineers decide the type of application that requires the hardness characteristics of AISI 1020 low carbon steel, selection of welding parameters and the material preparation process for optimal service performance.

2. Materials and Method

In this study, series of AISI 1020 low carbon steel weldments were produced by TIG welding process. Table 1 indicates the materials and specifications used for the welding process carried out in this study while the chemical composition of AISI 1020 are presented in Table 2.

Table 1: Materials and Specifications used for the TIG welding experiment

S/N	Material Specification	Welding Specification
1.	Filler Material	ER 70 S-6
2.	Joint Type	Butt Joint (V-groove)
3.	Joint Preparation	Abrasive Clean (Sand paper)/Acetone Wipe
4.	Welding Current	Direct Current Electrode Negative
5.	Pulse Width	0.8 Seconds
6.	Welding Torch Angle	45^o
7.	Torch Type	Pro-torch (TIG Torch)
8.	Tungsten Size	3/1326" Diameter x 25.4 mm
9.	Heat Input Ratio	10.75 KJ/min
10.	Weight of Filler Rod	78.5 Kg/m^2

Table 2: Chemical composition of AISI 1020 low carbon steel

S/N	Elements	Contents
1.	Carbon (C)	0.21%
2.	Iron (Fe)	98.7%
3.	Manganese (Mn)	0.78%
4.	Phosphorous (P)	0.02%
5.	Sulfur(S)	0.012%
6.	Silicon (Si)	0.14%
7.	Chromium (Cr)	0.03%
8.	Nickel (Ni)	0.03%
9.	Copper (Cu)	0.02%

AISI 1020 low carbon steel plate of 10 mm thickness each was cut into 120x30 mm (length x width) dimension as shown in Figure 1a. Emery paper (coarse: P24 grit size with 715 µm and fine: P80 grit size with 201 µm) was used to smoothen and eliminate rough particles and rust from the surface of specimen before welding as shown in Figure 1b. This was followed by cleaning the surface of the samples to be welded with acetone in order to eliminate surface contamination. Using vertical milling machine, the two steel plates were chamfered (2mm depth) with 30 degrees at the edge to form a V-groove angle while clamping it to a G-clamp. TIG welding was applied to join the plates and filling the chaffered region (see Figure 2) using 2% thoriated tungsten electrode. This was achieved through the use of Dynasty 210 DX welding machine and 100 % Argon as the torch gas to protect the welding region from contaminants.

(a)

(b)

Figure 1: Sample with v-groove showing unprepared surface and polished surface

(a)

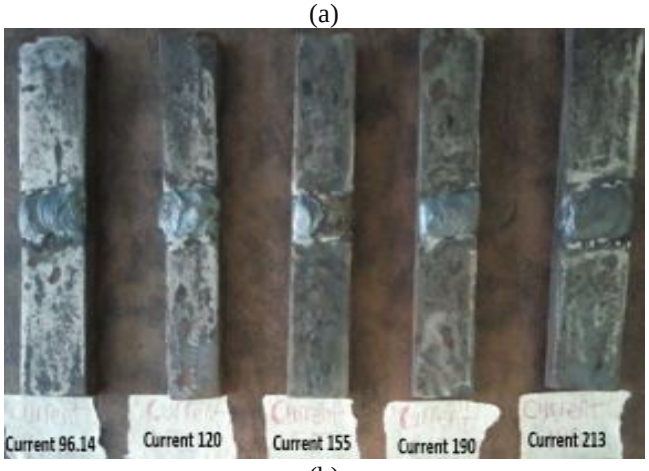

(b)

Figure 2: Prepared samples before and after welding

The electrode (2% thoriated tungsten electrode) was placed in the holder and the welding machine was turned on. The assembly was tack-welded to ensure alignment and an arc was struck. The weld was de-slagged, cleaned and welded again until the chamfered v-groove was filled to the same level with the surface of the specimens. After the final welding process, the specimen was allowed to cool on the floor at room temperature and subsequently a chipping hammer was used to remove the hard slag from the surface of the welds and the specimens were allowed to cool further. Analysis of the weldments of AISI 1020 low carbon steel plates was carried out to determine the microstructural properties and hardness characteristics with reference to the parent metal, HAZ, and the fusion zone. An alternating current supply was used in filling completely the V-Notch samples which maintained an arc gap of 2mm in between During welding, the plates were clamped properly to avoid unforeseen misalignments that may affect the quality of the welds. Table 3 presents the TIG welding input variables employed in the welding process.

Table 3: TIG welding input parameters

Weld Runs	Current (A)	Voltage (V)	Gas Flow Rate (L/min)
1	155	22	15.5
2	120	25	18
3	96.14	22	15.50
4	190	19	13
5	213	22	15.50

After welding, the welded samples were ground, polished, etched with Nital (ethanol nitric acid) and then visualized using SEM. The samples were illuminated by a reflected light which was mounted on the SEM equipment. The specimens were viewed with a scanning electron microscope through the eyepiece of the microscope, so as to determine the microstructure of the specimens. The structural images visualized for each sample were snapped by the camera attached to the SEM equipment to obtain the micrograph of the samples. This was viewed at a magnification of 100X. Applying a load of 150 kg and a dwell time of 10secs, hardness of the specimens was determined by the use of LECO micro-hardness tester. Hardness tests were performed on six (6) welded samples and their averages were recorded. The LECO micro-hardness tester evaluated the material hardness in Rockwell Hardness Number (HRC). The test was carried out on the welded samples at room temperature (27^{o}C). The hardness tests for the specimens were evaluated at three points as follows:

i. The fusion zone
ii. The heat affected zone
iii. The unaffected base metal

3. Results and Discussions

Scanning electron microscope was employed in examining the microstructure of the control and welded samples. Figure 3 represents microstructure of the control sample while Figures 4-8 reveal the microstructural views showing fusion zones and heat affected zones (HAZ) of TIG welded samples.

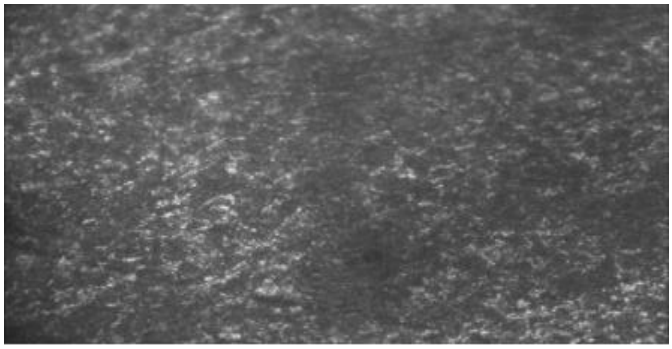

Figure 3: Control showing microstructure of the sample before welding

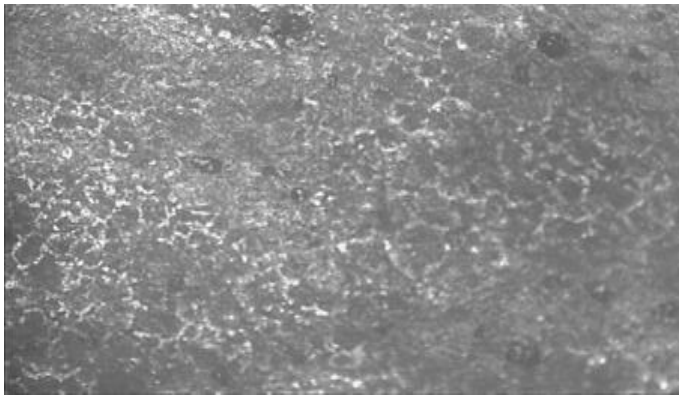

Figure 4a: Microstructure of sample showing fusion zone at welding current of 96.14A

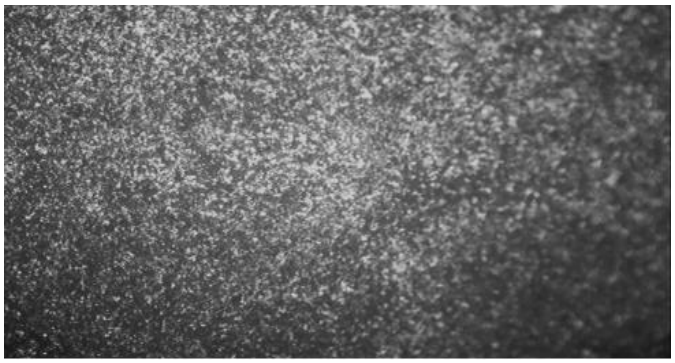

Figure 4b: Microstructure of sample showing HAZ at welding current of 96.14A

Figure 5a: Microstructure of sample showing fusion zone at welding current of 120A

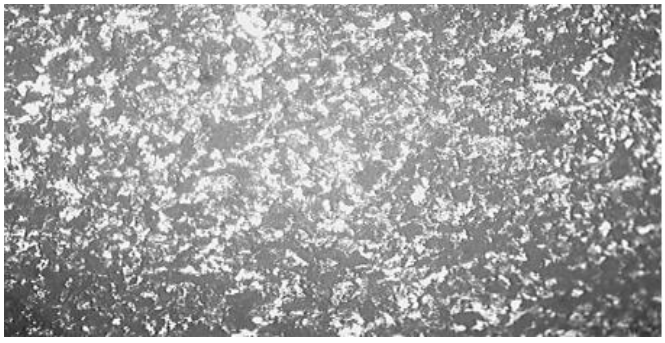

Figure 5b: Microstructure of sample showing HAZ at welding current of 120A

Figure 6a: Microstructure of sample showing fusion zones at welding current of 155A

Figure 6b: Microstructure of sample showing HAZ at welding current of 155A

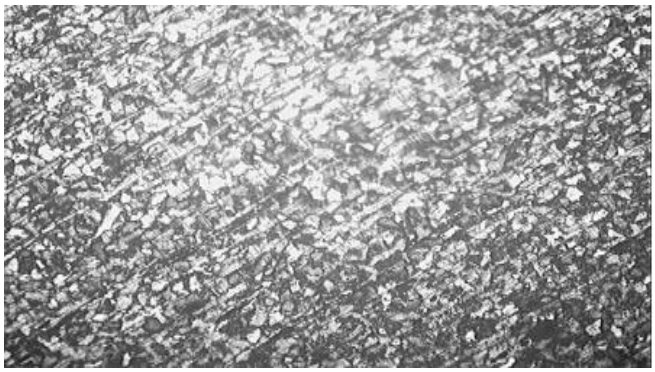

Figure 7a: Microstructure of sample showing fusion zones at welding current of 190A

Figure 7b: Microstructure of sample showing HAZ at welding current of 190A

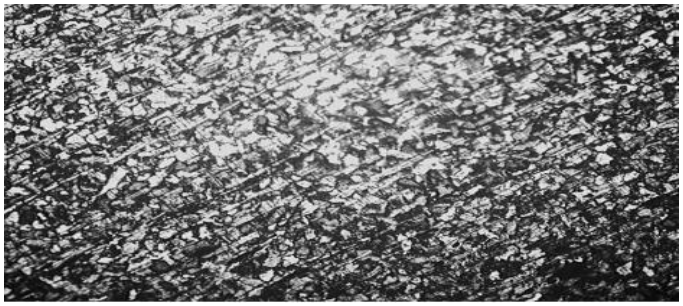

Figure 8a: Microstructure of sample showing fusion zones at welding current of 213A

Figure 8b Microstructure of sample showing HAZ at welding current of 213A

Figure 3 represents a control of the sample (parent metal without welding) indicating a very fine grains of ferrite and pearlite structures indicating high hardness of the specimen. Figure 4a represent microstructure of the welded sample, showing little increase in grain sizes of ferrite and pearlite as a result of heat inputs at a magnification of 100X. The hardness is high as a result of presence of fine grains. Malik et al. (2014) presented SEM micrograph of polished AISI 1020 low carbon steel specimens, which were characterized by fine grain ferritic and pearlitic structure. Figure 4b represents microstructure of the HAZ, indicating the presence of coarse grain ferrite and pearlite as result of heat effect, the hardness dropped when compared to the weldment at this heat input (see Figure 4a) at a magnification of 100X. Figure 5a represents the microstructure of welded sample, indicating the presence of coarse grains of ferrite and pearlite when compared to lower current (96.14 amp) resulting from heat input of weldment at 100X magnification. This indicates a decrease in hardness of weldment and increase in brittle failure. Figure 5b represents microstructure of the HAZ, indicating that the grains of ferrite and pearlite are coarser than that of (96.14 amp) at 100X magnification indicating decrease in hardness and increase in brittleness at HAZ. Figure 6a represents the microstructure of welded sample at current of 155 amp, indicating coarser grains of ferrite and pearlite compared to the fusion zone at welding current of 120 amp which indicated a step decrease in hardness at magnification of 100X. Figure 6b represents microstructure of HAZ at current of 155 amp, indicating coarse ferrite and pearlite when compared to (120 amp) sample HAZ, indicating decrease in hardness at a magnification of 100X. Figure 7a represents the microstructure of welded sample at current of 190 amp, indicating coarse grain structures of ferrite and pearlite when compared to (155A) weldment, decreasing hardness at 100X magnification. Figure 7b represents microstructure of HAZ at current of 190 amp, indicating coarser grains of ferrite and pearlite than weldment at 155 amp current as a result of heat increase in the HAZ indicating decrease in hardness at a magnification of 100X. Figure 8a represents the microstructure of welded sample at current of 213 amp, showing coarser grains of ferrite and pearlite than weldment at welding current 190 amp and indicating decrease in hardness when compared to weldment at current of 190 amp as a result of increased heat input at 100X magnification. Figure 8b represents microstructure of HAZ at current of 213amp, indicating coarser grains of ferrite and pearlite than HAZ at current of 190 amp and consequently decrease in hardness when compared to HAZ at welding current of 190 amp as a result of increase in heat input.

From the SEM micrographs presented in Figure 3-8, high hardness may be attributed to the fine grain size, needle shaped ferrite or the existence of widmanstatten inside ferrite grains (Abbaschian *et al.*, 2008) while lower hardness may be related to grain growth and the existence of ferrite (solid solution phase of carbon dissolved in alpha-iron) phase in the fusion zone and HAZ of the specimens as reported by Kacar & Kokemli (2005). For chemical composition of the AISI 1020 low carbon steel, Si and Mn are two of the most commonly occurring alloying elements that have a greater effect on the hardness of ferritic structure while Cr provides the least hardness increase. Silicon (Si) increases the hardness property of steel materials, but detrimental to surface quality particularly in low carbon steels, by aggravating crack tendencies when carbon content is fairly high. On the other hand, Manganese (Mn) significantly increase the hardenability of both steel but to a lesser extent than carbon. It reduces the cooling rate after welding, thereby, increasing the rate of hardenability of steel materials much more than any alloying element (Maalekian, 2007; Owunna and Ikpe, 2019).

As a result of stepwise increase in heat, hardness of the material decreased as the welding heat increased and the material hardness increased concurrently with the heat input. Hence, the material with lowest heat input had the highest hardness and can withstand load bearing capacity in service condition. This is because the grain size is finer with increasing hardness when compared to other samples with increasing heat input that has coarser grain particles/microstructure, as a result of intense operating thermal cycle and diffusion (Loureiro, 2002).

Microstructural characteristics of the welded samples with reference to cell spacing and the size of dendrites causes decreased in hardness of the post-weld joint are due to higher weld heat input, which is as a result of large dendrite particles as well as wide interdendritic spacing in the welded region. Therefore, hardness observed on the welds with large dendritic particle sizes and large interdendritic spacing in the region

welded were due to higher heat input. Thus, the application of higher heat inputs led to coarser microstructure of the welds.

Grain coarsening takes place as a result of operating thermal cycle and diffusion during the welding process. Grain particles located near the fusion point are exposed to higher temperature, causing the occurrence of grain growth around that region. Hence, larger grain sizes led to lower hardness values while hardness also decreased due to increase in the welding heat inputs. This agrees with the findings of Li *et al.* (2019) which revealed that after phase transformation in the fusion zone is completed, grains in the welded region becomes coarser with significant local embrittlement which reduces hardness performance of the welded steel material.

The factors that can influence the resultant hardness includes pre-heat, weld heat input, cooling rate, total thickness at the weld, alloying elements, alloy content of any flux and the original microstructural condition of the steel. The hardness can therefore be a useful indicator to determine if the thermal cycle induced by welding has rendered the heat affected zone (HAZ) adjacent to the weld susceptible to cracking or plastic deformation (Sultana *et al.*, 2014; Halilovic *et al.*, 2014).

The hardness value decreased with increasing welding current steps as shown in Figure 9, due to high heat inputs, and thus retention of heat in the fusion zone and HAZ. This occurred as a result of reduction in density of dislocation and microstructural coarsening. This may have also been due to slow cooling rate which presents nucleation of coarse grain structures with high intergranular spacing, thereby causing increase in grain dislocations within the crystal lattice of the fusion zone (Gharibshahiyan *et al.*, 2011). Dislocation in this context signifies a linear crystallographic defect of irregularity within a crystal structure that causes sudden change in the arrangement of atoms.

Grains close to the fusion line were exposed to higher thermal cycle and diffusion, therefore grain growth occurs. However, heat input around the fusion zone and HAZ of the welded specimen was enhanced by higher welding current as shown in Figure 9. This caused increase in grain sizes and decrease in hardness around the fusion zones and HAZ of the welded specimen. This correlated with the findings of Muda *et al.* (2015) which indicated that the higher the heat input, the coarser the microstructure. In addition to the findings, grain coarsening occurs due to operating thermal cycle and diffusion.

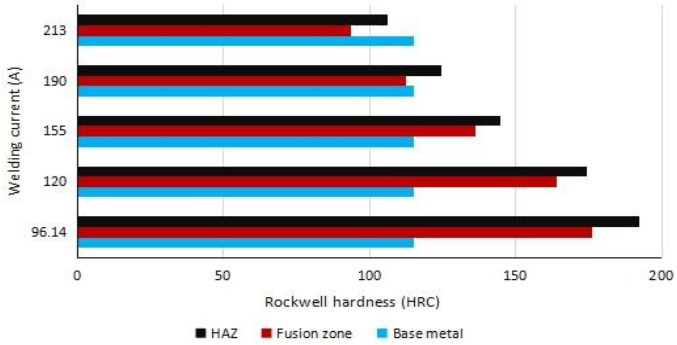

Figure 9: Effect of welding current on hardness properties of AISI 1020 carbon steel

Figure 9 represents the hardness profile for the test samples at different welding currents. It can be observed that the base metal maintains a uniform hardness profile for all the welding currents while a hardness variation is observed across the HAZ and the fusion zone. The variation (which causes deterioration of the material properties during service) is due to welding thermal cycle, semi-molten material reaching a maximum temperature, which depends on the distance from the fusion line, thereby, forming different microstructure after cooling (Liang *et al.*, 2015).

From Figure 9, it is observed that as the indenter travels from the mid-section of the welded region to the fusion boundary for each sample, the hardness properties decrease as the welding current inputs increases. The fusion zone has an average hardness value of 136.6 HRC, the base metal has hardness value of 115.2 HRC while the HAZ posed an average hardness of 148.5 HRC for welding currents specified in Figure 9. The reason for increase in hardness at the HAZ is due to fast cooling rate in a portion of the specimen adjacent to the welded region. This agrees with the findings of Rahul *et al.* (2014) which revealed that microstructure as well as micro-hardness are two parameters that depend on the cooling rate of weld metals, as faster cooling rate results in find grains with increased hardness while slower cooling rate causes the formation of coarse grains and reduction in hardness. In this case, a portion of the specimen adjoining the base plate is subjected to rapid cooling as a result of precipitous thermal gradients, causing a finer grain microstructure to be formed. The highest hardness is also due to the effectiveness of interstitial carbon atoms in hindering dislocation movement (as a solid-solution effect) and few slip of atoms along the latice of the weld (Callister, 2007). The arc heat generated in the welding process is due to increase in the welding current, causing the grain sizes to recrystallize and increase in size. Increase in grain size, reduces the hardness of the weld and that of the HAZ (Bodude and Momohjimoh, 2015). If the heat persists longer, it is transferred into the base plate due to low power density (the rate at which energy is transmitted per unit volume, area or mass) of the welding process as stated by Esquivel *et al.*, (2012). Furthermore, the base plate is affected as a result of intense heat transferred into the weld, thereby causing increase in the grain particles.

4. Conclusion

The findings of this study revealed that increase in welding current input caused more arc heat to be produced on the fusion line, resulting in expansion and contraction between the fusion zone and the base metal. This increased the residual stress in the weldment and heat affected zone which subsequently affected the hardness properties of AISI 1020 low carbon steel plate, thereby, causing a reduction in hardness around the fusion zone and HAZ of the material. With increased current, the heat generated increased proportionately causing the grains to recrystallized and grow in size. Increase in the grain sizes led to reduction in hardness value of the fusion zone and the heat affected zone, and were observed to occur with increasing welding heat inputs which reduced the hardness value. Therefore, higher heat input resulted in the formation of carbide precipitates along the grain boundaries, leading to sensitized zone around the grain boundaries which consequently caused

grain coarsening of the HAZ and decrease in hardness around that area. With increase in welding current, the arc heat increased and caused recrystallization of grain particles and increase in grain size. Higher welding heat input was also observed to be responsible for precipitation along the grain boundaries, causing sensitization of grain particles around the fusion zone and the HAZ. This played a vital role in grain coarsening of heat affected zones as well as reduction in hardness in that region and can cause poor performance of the weld during service conditions. Finally, low welding current implied low heat input which improved hardenability of the fusion zone and HAZ, were both characterized by fine grain microstructure in all the micrographs presented in this study.

References

Abbaschian, R., Abbaschan, L. and Reed-Hill, R. E. (2008). Physical Methology Principles. 4th Edition, Cengage Learning, Stamford, USA.

Badheka, V. J., Basu, R., Omale, J. and Szpunar, J. (2016). Microstructural Aspects of TIG and A-TIG Welding Process of Dissimilar Steel Grades and Correlation to Mechanical Behavior. Trans. of the Indian Institute of Metals, 16, 1-10.

Bodude, M. A. and Momohjimoh, I. (2015). Studies on Effects of Welding Parameters on the Mechanical Properties of Welded Low-Carbon Steel. Journal of Minerals and Materials Characterization and Engineering, 3, 142-153.

Callister, W.D. (2007). Materials Science and Engineering-An Introduction: USA, John Wiley and Sons, Inc.

Cibi, A. J. and Thilagham, K. T. (2017). High Frequency Gas Tungsten Arc Welding Process for Dressing of Weldment. Int'l Journal of Advanced Eng. Research & Sci., 4 (3), 229-35.

Esquivel, A. S., Nayak, S. S., Xia, M. S. and Zhou, Y. (2012). Microstructure, Hardness and Tensile Properties of Fusion Zone in Laser Welding of Advanced High Strength Steels. Canadian Metallurgical Quarterly, 51 (3), 328-335.

Gharibshahiyan, E., Raouf, A. H., Parvin, N. and Rahimian, M. (2011). The effect of Microstructure on Hardness and Toughness of Low Carbon Welded Steel Using Inert Gas Welding. Material and Design, 32(4), 2042-2048.

Halilovic, J., Butkovic, S., Mehmedovic, M. and Saric, M. (2014). Investigation of Hardness Profiles and Microstructure Change in the Weld Nugget and HAZ of Resistance Spot Welded Low Carbon Steel. 18th Int'l Research /Expert Conference, 10-12, 2014 TMT 2014, Budapest, Hungary.

Ikeh, O. D., Ikpe, A. E. and Njelle, V. Z. (2019). Effects of Electric Power Arc Inputs on the Fracture Surface and the Mechanical Properties of 0.4%C Steel. Journal of Science and Technology Research, 1 (3), 133-143.

Ikpe, A. E., Owunna, I. and Ememobong, I. (2017). Effects of Arc Voltage and Welding Current on the Arc Length of Tungsten Inert Gas Welding (TIG). International Journal of Engineering Technologies, 3 (4), 213-221.

Ishak, M., Noordin, N. F., Razali, A. S., Shah, L. H. and Romlay, F. R. (2015). Effect of Filler on Weld Metal Structure of Aa6061 Aluminum Alloy by Tungsten Inert Gas Welding. International Journal of Automotive and Mechanical Engineering, 11, 2438-2446.

Joshi, J. R., Potta, M., Adepu, K., Katta, R. K., Gankidi, M. R. (2016). A comparative evaluation of microstructural and mechanical behavior of fiber laser beam and tungsten inert gas dissimilar ultra-high strength steel welds. Defense Technology, 12, 464-472.

Kacar, R. and Kokemli, K. (2005). Effect of Controlled Atmosphere on the MIG-MAG Arc Weldment Properties. Materials and Design, 26(6), 508-516.

Kumar, A. and Sundarrajan, S. (2009). Effect of welding parameters on mechanical properties and optimization of pulsed TIG welding of Al-Mg-Si alloy. The Int'l Journal of Advanced Manufacturing Technology, 42, 118-125.

Li, D., Wu, K., Dong, H., Isayev, O. and Hress, O. (2019). Coarse Grained Heat-Affected Zone Microstructure and Brittleness of Ti-Nb-B Micro-alloyed High Toughness and Wear Resistant Steel. Metals, 9(289), 3-15.

Loureiro, A. J. (2002). Effect of Heat Input on Plastic Deformation of Under Matched Weld. Journal of Material Processing Technology, 128(1), 240-249.

Liang, Z., Qin, G., Wang, L., Meng, X. and Li, F. (2015). Microstructural Characterization and Mechanical Properties of Dissimilar Friction Welding of 1060 Aluminum to AZ31B. Material and Engineering A, 645, 170-180.

Maalekian, M. (2007). The Effects of Alloying Elements on Steels (I). Graz University of Technology, Styria, Austria.

Malik, J., Toor, I. H., Ahmed, W. H., Gasem, Z. M., Habib, M. A., Ben-Mansour, R. and Badr, H. M. (2014). Investigation on the Corrosion-Enhanced Erosion Behavior of Carbon Steel AISI 1020. Int'l Journal of Electrochemical Sci., 9, 6765-80.

Muda, W. S., Nasir, N. S., Mamat, S. and Jamian, S. (2015). Effect of Welding Heat Input on Microstructure and Mechanical Properties at Coarse Grain Heat Affected Zone of ABS Grade A Steel. ARPN Journal of Engineering and Applied Sciences, 10(20), 9487-9495.

Rahul, G., Arya, H. K. and Saxena, R. K. (2014). Effect of Cooling Rate on Microstructure of Saw Welded Mild Steel Plate (Grade C 25 as per IS 1570). International Journal of Modern Engineering Research, 4 (1), 222-228.

Owunna, I. B. and Ikpe, A. E. (2019). Modelling and Prediction of the Mechanical Properties of TIG Welded Joint for AISI 4130 Low Carbon Steel Plates Using Artificial Neural Network (ANN) Approach. Nigerian Journal of Tech., 38 (1), 117-126.

Ravichandran, M., Sait, A. N. and Vignesh, U. (2017). Investigation on TIG welding parameters of 2205 duplex stainless steel. International Journal of Automotive and Mechanical Engineering, 14 (3), 4518-4530.

Singh, A., Singh, J. and Kumar, R. (2016). A Study of Microstructure and Hardness in En 31steel and Mild Steel Welded Joints Using TIG Welding. International Journal of Engineering Science and Computing, 6 (10), 2849- 2854.

Srirangan, A. K. and Paulraj, S. (2015). Multi-response Optimization of Process Parameters for TIG Welding of Incoloy 800HT by Taguchi Grey Relational Analysis. Eng. Sci. & Technology, Int'l Journal, 19 (2), 811-817, 2015.

Sultana, M. N., Hasan, M, F. and Islam, M. (2014). Analysis of Mechanical Properties of Mild Steel Applying Various Heat Treatment. Int'l Conference on Mechanical, Industrial & Energy Engineering, 25-26, Khulna, Bangladesh.

Uduehiabhulimen, I. (2014). Evaluation of the Hardness and Microstructure of a Tungsten Inert Gas Weld of a Mild Steel Pipe Joint. International Journal of Research in Engineering and Technology, 2 (8), 117-126